Time-Resolved Measurements of Hot-Electron Equilibration Dynamics in High-Intensity Laser Interactions with Thin-Foil Solid Targets

High-intensity laser interactions with solid targets generate extreme states of matter[1] with unique energy-transport properties.[2,3] At laser intensities above 10^{18} W/cm^2, high-current electron beams with ~MeV energies are generated,[4–7] heating matter to high thermal temperatures over picosecond time scales.[2,3,8] Understanding the energy partition and its evolution in these highly nonequilibrium plasmas is an important open issue, underpinning applications in high-energy-density science,[1] plasma-based particle acceleration,[9] warm, dense matter,[10] high-peak-power γ-ray generation,[11] and advanced inertial fusion energy concepts, including fast ignition.[12] In these conditions, the hot-electron equilibration dynamics are not completely understood, and accurate time-resolved measurements are required to test energy partition and temperature equilibration models.

The only previous hot-electron equilibration data in this regime are the time-resolved K_α-emission data of Chen *et al.*[13] In these experiments thin-foil targets were irradiated with ~0.5-ps pulses focused to intensities up to 10^{19} W/cm^2, and the K_α-emission pulse width was used to characterize the time scale for energy thermalization ("relaxation") between hot and cold electrons. The data showed K_α-emission pulse widths from ~12 to 16 ps. The data were compared to an electron-energy–transfer model that included ion-front expansion and collisional electron-energy transfer based on the Landau–Spitzer theory.[14] With increasing laser intensity, the model did not reproduce the rise time (~10 ps) or the duration of the measured K_α signals, revealing an incomplete picture of the hot-electron equilibration dynamics.

In this article, ultrafast measurements of the hot-electron relaxation time in high-intensity laser–solid interactions are reported. Thin-foil targets were irradiated with 0.5- to 1-ps pulses focused to intensities from ~10^{18} to 10^{19} W/cm^2 and the hot-electron equilibration dynamics studied with time-resolved K_α spectroscopy. In these interactions, the full width at half maximum (FWHM) of the K_α signal increased with laser intensity from ~3 to 6 ps. These are the first experiments at relativistic laser intensities to show rapid hot-electron relaxation times with K_α-emission pulse widths up to a factor of 4× shorter than in previously reported experiments.[13] To provide insight into the mean energy of the hot electrons contained inside the target, the duration of the measured K_α signals were compared to predictions from a collisional energy-transfer model. Assuming collisional energy transfer dominates, the data suggest that hot electrons with mean energies from ~0.8 to 2 MeV are contained inside the target. The inferred mean hot-electron energies are broadly consistent with ponderomotive scaling[6] over the relevant intensity range.

The experiments were carried out with LLE's Multi-Terawatt (MTW) laser.[15] Figure 129.18 shows a schematic of the experimental setup. The MTW laser delivered 1- to 10-J, 0.5- to 1-ps pulses at a wavelength of 1.053 μm that were focused by an f/3 off-axis parabolic mirror to a spot with a FWHM of ~5 μm, providing vacuum-focused intensities from ~10^{18} to 10^{19} W/cm^2. The laser-intensity contrast was ~10^8 at 100 ps before the peak of the main laser pulse.[16] The laser was focused at normal incidence on 500 × 500 × 20-μm^3 Cu-foil targets mounted on 17-μm-diam silicon carbide stalks.

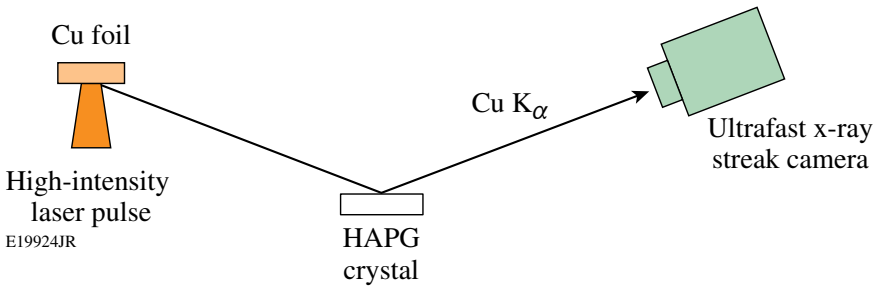

Figure 129.18
Experimental setup. HAPG: highly annealed pyrolytic graphite.

Time resolving the K_α radiation generated in these experiments is a direct technique for inferring the hot-electron relaxation time.[13] K_α radiation emitted from the target was measured with a 2-ps time-resolution x-ray streak camera[17] coupled to a HAPG (highly annealed pyrolytic graphite) crystal spectrometer. The HAPG crystal was toroidally curved and collected radiation from 7.8 to 8.5 keV. This spectral range covers the $2p \rightarrow 1s$ transition in Cu, allowing for time-resolved Cu K_α measurements at 8.05 keV.

The streak camera was independently characterized by direct illumination of the photocathode with a 10-mJ, 0.5-ps pulse of 263-nm light. Figure 129.19 shows a schematic of the setup. By passing half of the UV beam through a quartz plate of known thickness, two pulses were generated, providing a sweep-speed calibration. Figure 129.19(b) shows a typical streak-camera trace for these two pulses. The pulse widths (FWHM) are 1.8±0.1 and 1.9±0.1 ps. Temporal dispersion in the streak camera gives a slightly different impulse response for x-ray illumination. Monte Carlo modeling of the electron optics inside the streak tube shows that this offset is ~0.2 ps, giving an impulse response for x rays of ~2 ps.

Figure 129.20 shows an example of time-resolved plasma x-ray emission data for different high-intensity laser irradiation conditions. Figure 129.20(a) shows the time-resolved K_α emission from a $500 \times 500 \times 20$-μm^3 Cu foil irradiated with a 0.9-J, 0.6-ps pulse focused to 3.6×10^{18} W/cm^2. The pulse width is 3.0±0.2 ps. Figure 129.20(b) shows the K_α emission from a similar target irradiated with an 8.5-J, 0.8-ps pulse focused to 2.9×10^{19} W/cm^2. The pulse width is 5.5±0.1 ps. The K_α emission from these targets was measured as a peaked signal with a sharp rise and a slower decay. The signal rise time did not vary with laser intensity and was determined by the experimental resolution. The signal decay time increased with laser intensity and was sensitive to the hot-electron equilibration dynamics.

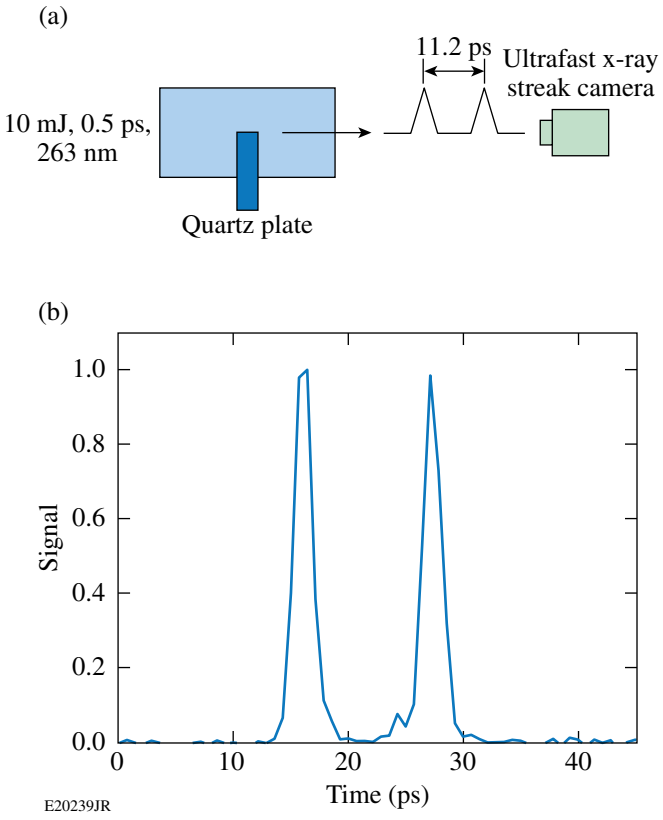

Figure 129.19
(a) Streak-camera calibration setup. (b) Streak-camera response measurement with 0.5-ps, 263-nm pulses showing pulse widths of 1.8±0.1 and 1.9±0.1 ps.

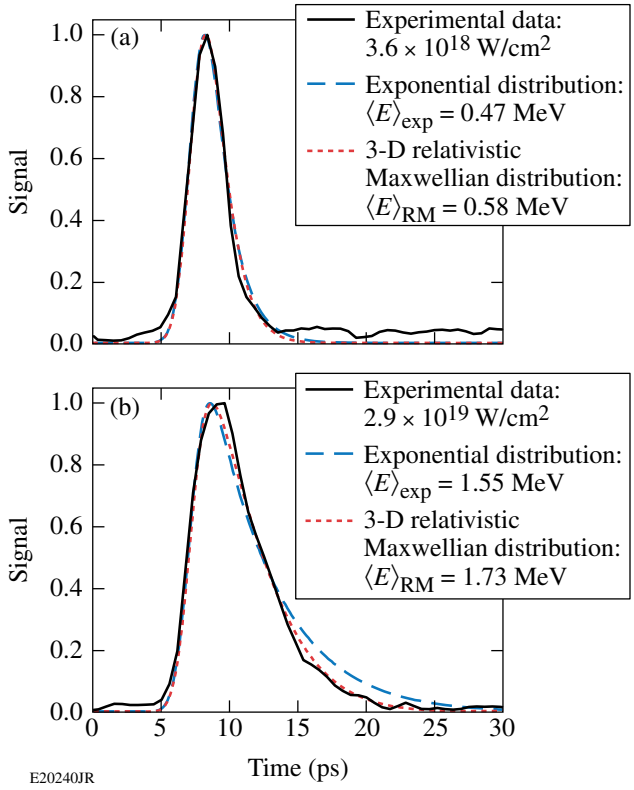

Figure 129.20
Experimental time-resolved K_α emission data from $500 \times 500 \times 20$-μm^3 Cu foils. The targets were irradiated with (a) a 0.9-J, 0.6-ps pulse and (b) an 8.7-J, 0.8-ps pulse. The data are shown with theoretical fits based on a collisional energy-loss model with exponential (blue dashed line) and 3-D relativistic Maxwellian (red dashed line) hot-electron energy distributions.

K_α radiation was generated in these experiments by hot electrons that were confined by target charging.[7,18,19] The thin-foil targets rapidly charge because of the electrostatic potential that develops after the initial loss of a small fraction of high-energy electrons.[18] The remaining hot electrons (>90% of the total laser-accelerated population) make multiple round-trips of the target as they recirculate (reflux) because their collisional range is several hundred microns at solid density.[20]

A collisional energy-loss model for understanding hot-electron relaxation and the time dependence of K_α emission in these targets has been developed. The model calculates the K_α emission rate for a given hot-electron energy distribution, assuming that all of the electrons are trapped inside the foil. The hot-electron energy loss rate is given by[20]

$$\frac{\mathrm{d}E}{\mathrm{d}t} = -\frac{n_\mathrm{e} e^4 L_\mathrm{d}}{4\pi\epsilon_0^2 m_\mathrm{e} v}, \tag{1}$$

where n_e is the electron density for solid Cu (2.46×10^{24} cm^{-3}), E is the hot-electron energy, m_e is the electron rest mass, v is the hot-electron velocity, e is the electron charge, and ϵ_0 is the permittivity of free space. The stopping number L_d (or "log Λ") depends weakly on material and the hot-electron energy, with values for Cu taken from Ref. 21. The time spent by hot electrons outside the target during recirculation is assumed negligible, and energy losses to ion acceleration and self-generated electric fields are not considered in this model.[7,18,19]

K_α-emission pulse widths have been calculated for hot electrons with exponential

$$\left(f_\mathrm{h} \propto e^{-\gamma m_\mathrm{e} c^2 / k_\mathrm{B} T_\mathrm{h}}\right)$$

and three-dimensional relativistic Maxwellian

$$\left[f_\mathrm{h} \propto \gamma\left(\gamma^2 - 1\right)^{1/2} e^{-\gamma m_\mathrm{e} c^2 / k_\mathrm{B} T_\mathrm{h}}\right]$$

energy distributions, where k_B is Boltzmann's constant, T_h is the hot-electron temperature, and γ is the Lorentz factor. Isochoric energy transfer to solid matter in these calculations is assumed. The K_α-emission rate is proportional to the Cu ion density, the time-varying number of hot electrons, and the parameter $\langle \sigma_\mathrm{K} v \rangle$ averaged over the hot-electron energy distribution, where σ_K is the K-shell ionization cross section and v is the hot-electron velocity. The cross section for ionization of K-shell electrons was taken from Ref. 21.

Figure 129.20 shows synthetic K_α streaks that were calculated from this model. The synthetic pulse widths represent a convolution of the calculated K_α-emission rate with the laser pulse duration and the temporal resolution of the x-ray streak camera. In the low-intensity case [Fig. 129.20(a)], the model predicts well the K_α emission pulse shape, independent of the hot-electron energy distribution that was used. The best fit of the experimental data was obtained with the parameters $\langle E \rangle_\mathrm{exp} = 0.47$ MeV for the exponential energy distribution and $\langle E \rangle_\mathrm{RM} = 0.58$ MeV for the three-dimensional (3-D) relativistic Maxwellian energy distribution. In the high-intensity case [Fig. 129.20(b)], the best fit was obtained with the parameters $\langle E \rangle_\mathrm{exp} = 1.55$ MeV and $\langle E \rangle_\mathrm{RM} = 1.73$ MeV. In this case, the K_α-emission pulse shape was better reproduced by model calculations with a 3-D relativistic Maxwellian energy distribution.

Figure 129.21 shows the variation with increasing laser intensity of the measured K_α emission pulse width. An upper estimate of the true K_α-emission pulse width was obtained by accounting for instrumental effects, subtracting the FWHM of the impulse response function from the streak-camera trace in quadrature. Gaussian pulse shapes are assumed. For laser intensities between 2.7×10^{18} and 3.4×10^{19} W/cm^2, the duration of the measured K_α signal increases from ~3 to 6 ps. Over this intensity range, the K_α-emission pulse width increases with

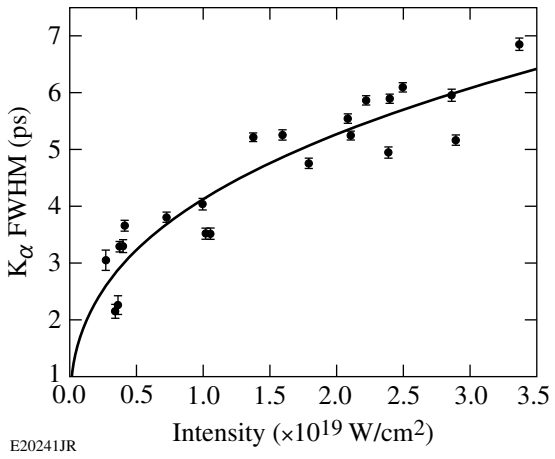

Figure 129.21
Experimental K_α-emission pulse width as a function of laser intensity. The pulse widths have been adjusted to account for the impulse response of the streak camera.

laser intensity and is given by $\tau_{K_\alpha}[\text{ps}] = (4.1 + 0.3) I_{19}^{0.35\pm0.07}$, where I_{19} is the laser intensity in units of 10^{19} W/cm^2.

To obtain a mean hot-electron energy scaling, these data are compared with the collisional energy-loss model. Figure 129.22(a) shows the relationship between the calculated K_α-emission pulse width and the mean hot-electron energy for exponential and 3-D relativistic Maxwellian energy distributions. In these calculations, the K_α-emission rate was convolved with a 0.8-ps FWHM Gaussian pulse that approximated the range of laser pulse durations that were used in these experiments. The synthetic pulse was convolved with a 2-ps FWHM Gaussian instrument response that was removed in quadrature for comparison with the experimental data (Fig. 129.21). Figure 129.22(a) shows that calculations with a 3-D relativistic Maxwellian energy distribution have slightly higher mean hot-electron energies than with an exponential energy distribution for a given K_α-emission pulse width. This offset is ~100 to 200 keV.

Figure 129.22(b) shows the mean hot-electron energies that are inferred from the experimental data based on this model. Two scaling laws were obtained: For an exponential energy distribution, $\langle E \rangle_{\text{exp}}[\text{MeV}] = (1.12\pm0.11) I_{19}^{0.51\pm0.11}$. For a 3-D relativistic Maxwellian energy distribution, $\langle E \rangle_{\text{RM}} = [\text{MeV}] = (1.19\pm0.11) I_{19}^{0.46\pm0.10}$. Assuming collisional energy transfer dominates, these results show that mean hot-electron energies from ~0.8 to 2 MeV are required to generate K_α-emission pulse widths consistent with the experimental observations.

Figure 129.22(c) compares these inferred mean hot-electron energies with ponderomotive scaling.[6] Ponderomotive scaling gives

$$\langle E \rangle = m_e c^2 \left[1 + \left(2U_p / m_e c^2 \right) \right]^{1/2},$$

where $U_p = 9.33 \times 10^{-14} I\,[\text{W/cm}^2]\,(\lambda\,[\mu\text{m}])^2$ is the ponderomotive potential. In general, good agreement was found. The best agreement was found for calculations with an exponential energy distribution. A similar scaling predicting ~100- to 200-keV-higher mean hot-electron energies was found with calculations using the 3-D relativistic Maxwellian energy distribution.

Including the energy-transfer model energy loss to self-generated fields and ion acceleration would increase the inferred mean hot-electron energy and lead to a faster increase in the K_α-emission pulse width with laser intensity since these effects are expected to be greater at higher intensities. In the limit of isochoric energy transfer, additional energy loss mechanisms will increase the mean hot-electron energy required to gen-

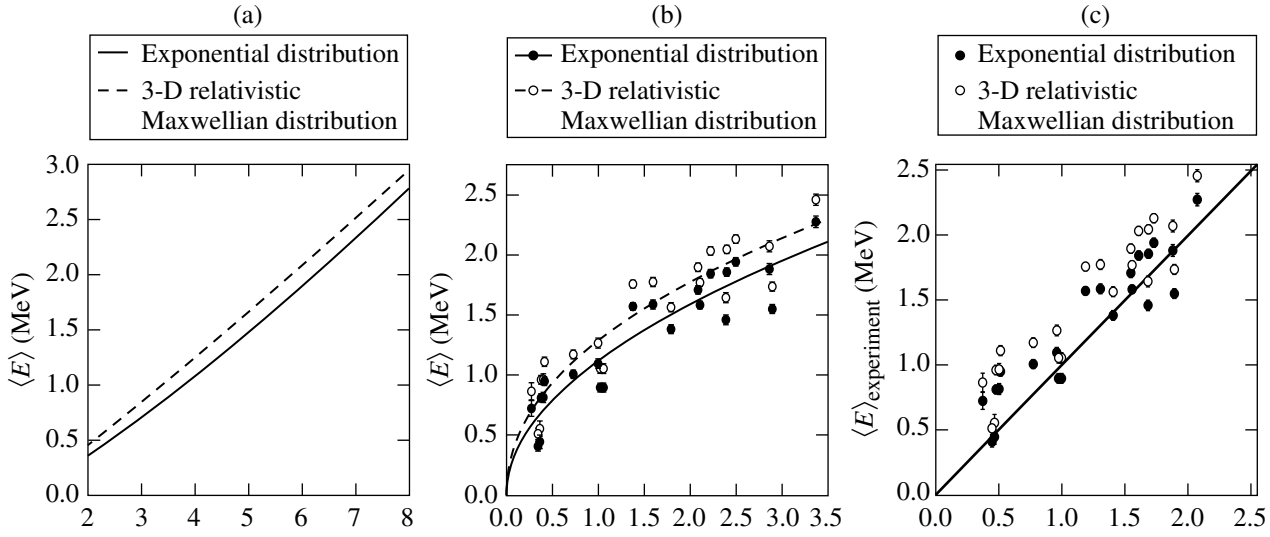

Figure 129.22
(a) Calculated mean hot-electron energy $\langle E \rangle$ as a function of K_α-emission pulse width based on a 0.8-ps laser-pulse duration. (b) Inferred $\langle E \rangle$ as a function of laser intensity, assuming exponential (solid line) and 3-D relativistic Maxwellian (dashed line) hot-electron energy distributions. (c) Comparison of the experimentally inferred $\langle E \rangle$ with ponderomotive scaling.[6]

erate the experimentally observed K_α emission. These results represent a minimum value for the inferred mean hot-electron energy required to generate the experimentally observed K_α-emission pulse widths.

In summary, the hot-electron equilibration dynamics in thin-foil solid targets irradiated with high-intensity laser pulses have been studied. Time-resolved K_α spectroscopy measurements show K_α-emission pulse widths from ~3 to 6 ps for laser intensities between ~10^{18} and 10^{19} W/cm^2. Assuming collisional energy transfer dominates, the experimental data suggest that hot electrons with mean energies from ~0.8 to 2 MeV are contained inside the target. The inferred mean hot-electron energy scaling with laser intensity is broadly consistent with ponderomotive scaling. These findings are important for the understanding of a wide range of high-energy-density physics applications that require a large and fast energy input into matter.

ACKNOWLEDGMENT

This work was supported by the U.S. Department of Energy Office of Inertial Confinement Fusion under Cooperative Agreement No. DE-FC52-08NA28302, the University of Rochester, and the New York State Energy Research and Development Authority. The support of DOE does not constitute an endorsement by DOE of the views expressed in this article.

REFERENCES

1. B. A. Remington *et al.*, Science **284**, 1488 (1999).
2. J. A. Koch *et al.*, Phys. Rev. E **65**, 016410 (2001); K. Eidmann *et al.*, J. Quant. Spectrosc. Radiat. Transf. **81**, 133 (2003); P. Audebert *et al.*, Phys. Rev. Lett. **94**, 025004 (2005).
3. C. R. D. Brown *et al.*, Phys. Rev. Lett. **106**, 185003 (2011).
4. D. F. Price *et al.*, Phys. Rev. Lett. **75**, 252 (1995); H. Chen, B. Soom, B. Yaakobi, S. Uchida, and D. D. Meyerhofer, Phys. Rev. Lett. **70**, 3431 (1993); K. B. Wharton *et al.*, Phys. Rev. Lett. **81**, 822 (1998); K. Yasuike *et al.*, Rev. Sci. Instrum. **72**, 1236 (2001); S. P. Hatchett *et al.*, Phys. Plasmas **7**, 2076 (2000).
5. F. N. Beg *et al.*, Phys. Plasmas **4**, 447 (1997).
6. S. C. Wilks *et al.*, Phys. Rev. Lett. **69**, 1383 (1992).
7. P. M. Nilson, A. A. Solodov, J. F. Myatt, W. Theobald, P. A. Jaanimagi, L. Gao, C. Stoeckl, R. S. Craxton, J. A. Delettrez, B. Yaakobi, J. D. Zuegel, B. E. Kruschwitz, C. Dorrer, J. H. Kelly, K. U. Akli, P. K. Patel, A. J. Mackinnon, R. Betti, T. C. Sangster, and D. D. Meyerhofer, Phys. Rev. Lett. **105**, 235001 (2010).
8. A. Saemann *et al.*, Phys. Rev. Lett. **82**, 4843 (1999); P. Audebert *et al.*, Phys. Rev. Lett. **89**, 265001 (2002).
9. E. L. Clark *et al.*, Phys. Rev. Lett. **84**, 670 (2000); R. A. Snavely *et al.*, Phys. Rev. Lett. **85**, 2945 (2000).
10. P. K. Patel *et al.*, Phys. Rev. Lett. **91**, 125004 (2003).
11. P. A. Norreys *et al.*, Phys. Plasmas **6**, 2150 (1999).
12. M. H. Key, M. D. Cable, T. E. Cowan, K. G. Estabrook, B. A. Hammel, S. P. Hatchett, E. A. Henry, D. E. Hinkel, J. D. Kilkenny, J. A. Koch, W. L. Kruer, A. B. Langdon, B. F. Lasinski, R. W. Lee, B. J. MacGowan, A. MacKinnon, J. D. Moody, M. J. Moran, A. A. Offenberger, D. M. Pennington, M. D. Perry, T. J. Phillips, T. C. Sangster, M. S. Singh, M. A. Stoyer, M. Tabak, G. L. Tietbohl, M. Tsukamoto, K. Wharton, and S. C. Wilks, Phys. Plasmas **5**, 1966 (1998); M. Tabak *et al.*, Phys. Plasmas **1**, 1626 (1994).
13. H. Chen *et al.*, Phys. Rev. E **76**, 056402 (2007).
14. L. D. Landau, Phys. Z. Sowjetunion **10**, 154 (1936); L. Spitzer, *Physics of Fully Ionized Gases*, 2nd rev. ed., Interscience Tracts on Physics and Astronomy (Wiley Interscience, New York, 1962).
15. V. Bagnoud, I. A. Begishev, M. J. Guardalben, J. Puth, and J. D. Zuegel, Opt. Lett. **30**, 1843 (2005).
16. V. Bagnoud, J. D. Zuegel, N. Forget, and C. Le Blanc, Opt. Express **15**, 5504 (2007).
17. C. Stoeckl, W. Theobald, P. A. Jaanimagi, P. Nilson, M. Storm, J. A. Delettrez, R. Epstein, T. C. Sangster, D. Hey, A. J. MacKinnon, H.-S. Park, P. K. Patel, R. Shepherd, J. Green, K. L. Lancaster, and P. A. Norreys, Bull. Am. Phys. Soc. **52**, 67 (2007).
18. J. Myatt, W. Theobald, J. A. Delettrez, C. Stoeckl, M. Storm, T. C. Sangster, A. V. Maximov, and R. W. Short, Phys. Plasmas **14**, 056301 (2007).
19. A. J. Mackinnon *et al.*, Phys. Rev. Lett. **88**, 215006 (2002); Y. Sentoku *et al.*, Phys. Plasmas **10**, 2009 (2003); W. Theobald, K. Akli, R. Clarke, J. Delettrez, R. R. Freeman, S. Glenzer, J. Green, G. Gregori, R. Heathcote, N. Izumi, J. A. King, J. A. Koch, J. Kuba, K. Lancaster, A. J. MacKinnon, M. Key, C. Mileham, J. Myatt, D. Neely, P. A. Norreys, H.-S. Park, J. Pasley, P. Patel, S. P. Regan, H. Sawada, R. Shepherd, R. Snavely, R. B. Stephens, C. Stoeckl, M. Storm, B. Zhang, and T. C. Sangster, Phys. Plasmas **13**, 043102 (2006); S. D. Baton *et al.*, High Energy Density Phys. **3**, 358 (2007); P. M. Nilson, W. Theobald, J. Myatt, C. Stoeckl, M. Storm, O. V. Gotchev, J. D. Zuegel, R. Betti, D. D. Meyerhofer, and T. C. Sangster, Phys. Plasmas **15**, 056308 (2008); P. M. Nilson, W. Theobald, J. F. Myatt, C. Stoeckl, M. Storm, J. D. Zuegel, R. Betti, D. D. Meyerhofer, and T. C. Sangster, Phys. Rev. E **79**, 016406 (2009).
20. H. O. Wyckoff, *ICRU Report*, International Commission on Radiation Units and Measurements, Inc., Bethesda, MD (1984).
21. J. P. Santos, F. Parente, and Y.-K. Kim, J. Phys. B: At. Mol. Opt. Phys. **36**, 4211 (2003).